ICCSPA20 1570622270

On the Performance of Downlink NOMA Systems over Hyper-Rayleigh Fading Channels

M. Al-Jarrah
School of Electrical and Electronic Engineering
University of Manchester
Manchester M13 9PL, U.K.
Email: mohammad.al-jarrah@manchester.ac.uk

A. Aldweik
Center for Cyber Physical Systems
Khalifa University
Abu Dhabi, P.O.Box 127788, UAE.
Email: arafat.dweik@ku.ac.ae

E. Alsusa
School of Electrical and Electronic Engineering
University of Manchester
Manchester M13 9PL, U.K.
Email: e.alsusa@manchester.ac.uk

***Abstract*— This paper presents the bit error rate (BER) evaluation of downlink power-domain nonorthogonal multiple access (NOMA) systems in hyper-Rayleigh fading channels. Hyper-Rayleigh models perfectly captures the fading scenarios in which few number of strong components dominate the received signal strength. In addition, the order statistics model is applied to capture the difference in distance between the basestation and users. The transmitted signals of all users are modulated using phase shift keying (PSK), and then multiplexed at the basestation using power-domain NOMA. The well-known successive interference cancellation (SIC) detection is applied at the receivers' side to recover the information signals. Because hyper-Rayleigh models do not generally have closed form expressions, and due to the randomly located discontinuity in the amplitude probability density function (PDF), Monte Carlo simulation is used to evaluate the BER where 10^7 symbols are generated per simulation run. The obtained results show that hyper-Rayleigh fading may severely degrade the system BER at high signal-to-noise ratios (SNRs) as compared to Rayleigh channels. However, the Rayleigh fading seems to cause higher BERs at low SNRs.**

I. Introduction

There is no doubt that the introduction of the fifth generation (5G) communication networks has managed to increase the network capacity, reduce the delay, and provide higher data rates as compared to fourth generation (4G) networks. Nevertheless, the demand for extra capacity and higher data rates is continuously increasing, which maintains the pressure for the design of more efficient networks. For example, while the mobile data traffic in North America is about 9 GB per month in 2019, it is expected to hike up to about 45 GB per month, as anticipated by Ericsson [1]. Therefore, extensive research will remain focused on capacity enhancement technologies such as massive multiple-input-multiple-output (mMIMO) [2], network densification [3], network virtualization [4]–[6], millimeter wave communications [7], free-space optical (FSO) and visible light communication (VLC) [8], [9], and nonorthogonal multiple access (NOMA), which has been considered extensively in the recent literature [10]–[21].

In conventional orthogonal multiple access (OMA), a dedicated resource element in the form of time, frequency, space, or code is assigned to each user. Although OMA can effectively eliminate the inter-user interference (IUI), it does not provide sufficient spectral efficiency, which is highly desired for most applications. Consequently, NOMA has been introduced as a solution for increasing the capacity of future cellular networks by allowing multiple users to share the same resource element [21]. However, the increase in network capacity is obtained at the expenses of more complex receivers to mitigate the IUI, and higher bit error rate (BER) values [17]–[20].

The IUI caused by nonorthogonal transmissions can be controlled in the power or code domains. In power-domain NOMA, multiple users share the same resource element by assigning different transmission power for each user to enable demultiplexing the signal of each user. In code-domain NOMA, spreading sequences are applied at the basestation (BS), where these sequences have typical properties such as sparsity, low-density and low correlation. At the receiver side, i.e., users' equipment in the downlink scenario, successive interference cancellation (SIC) can be applied to demultiplex and detect the signal for each user. Accordingly, the nth user detects the signals of users 1, 2,. . ., $n-1$, and subtracts them from the received signal before extracting its own symbols [17]–[20].

It is worth noting that most of the work reported in the literature about NOMA considers the analysis of the capacity [10]–[13] and outage probability (OP) [14]–[16], whereas a few researchers have considered the bit error rate (BER) analysis [17]–[20]. For example, the authors in [12] introduced a comparison between the capacity of MIMO-NOMA and MIMO-OMA. Power allocation algorithms are proposed in [10] to maximize the ergodic capacity of MIMO-NOMA systems. The capacity of NOMA based cooperative relaying systems is analyzed in [11], and a capacity scaling scheme is proposed in [13] for device-to-device cooperative relaying. In [14], a dynamic power allocation algorithm in proposed for hybrid NOMA systems, and the OP is derived. Moreover, the OP with statistical channel state information (CSI) is derived in [15], whereas imperfect CSI is considered in [16]. The BER analysis of NOMA-based systems has received increased

[1]978-1-7281-6535-6/20/$31.00 ©2020 IEEE

attention in the recent literature [17]–[20]. The pairwise error probability (PEP) of NOMA based systems over Nakagami-m fading channels is analyzed in [17], whereas closed form expressions for BER are provided in [20]. Derivations for the error probabilities of space shift keying (SSK) based NOMA, and NOMA-based relay networks with simultaneous wireless information and power transfer (SWIPT) systems are provided in [18], and [19], respectively.

Although the Nakagami-m and Rayleigh are widely used to model wireless channels in urban and suburban scenarios, such channel models are typically not accurate in rural scenarios, where the number of reflected multipath components is very small [22], [23], which corresponds to hyper-Rayleigh fading channels. Therefore, this paper aims at evaluating the BER of NOMA systems in hyper-Rayleigh fading channels, which is to the best of the authors' knowledge, has never been considered in the literature. The channel is modeled as an ordered hyper-Rayleigh to capture both the small and large fading effects of the wireless channels. The obtained simulation results show that the BER of NOMA systems is drastically different from the case of Rayleigh fading, and from the case of single-user scenarios. More specifically, the results show that the BERs of the Rayleigh and hyper-Rayleigh intersect at certain SNR values, which implies that each fading model will be more severe than the other in a certain SNR range.

The rest of the article is organized as follows. Sections II and III introduce the system and fading channel models, respectively. The SIC based detector is discussed in Section IV. Simulation results are presented in Section V. Finally, the conclusion is provided in Section VI.

II. System and Channel Models

A. Transmitter Model

In this work, power-domain downlink NOMA system is considered with a single antenna BS and single antenna N users, U_1, ..., U_N. The BS multiplexes the N signals in power domain, to generate a multiuser signal, by assigning each user a different transmission power. Then, composite signal is transmitted to all users over the same resource element. Therefore, the multiuser signal transmitted from the BS can be expressed as

$$x = \sum_{n=1}^{N} \sqrt{\beta_n P_T} s_n \tag{1}$$

where s_n is the nth user's data symbol picked from a Gray coded PSK constellation, P_T is the total transmission power, and β_n is the allocated power coefficient for the nth user, i.e., $\sum_{n=1}^{N} \beta_n = 1$. Fig. 1 shows an example for the resultant composite symbol constellation for $N = 2$, where both users apply quadrature PSK (QPSK) and the bits of the first user, i.e., far user, are the most left two bits. In this case, the inphase and quadrature components of the multiplexed signal x, i.e., $x_I \triangleq \Re(x)$ and $x_Q \triangleq \Im(x)$, can be written as [20],

$$A_{u_1 u_2} = u_1 \sqrt{\beta_1} + u_2 \sqrt{\beta_2},\ u_i \in \{1, -1\}. \tag{2}$$

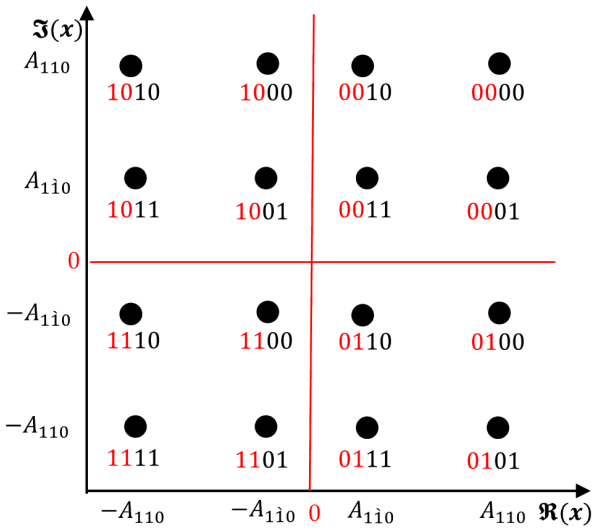

Fig. 1. The constellation diagram of the superimposed symbol x for $N = 2$, [20].

As can be observed from the figure, the superimposed NOMA symbol x is similar to a 16 quadrature amplitude modulation (16 QAM) constellation with modulation order $M = 16$.

B. Channel Model

The transmission medium in wireless communication systems is typically subject to multipath fading, where multiple copies of the transmitted signal are received at the destination with different time delays, frequency offsets, and amplitudes. The overall effect of the multipath phenomenon depends on the environment where the transmitter and receiver are located, which is widely modeled as Rician or Rayleigh fading. In such models, it is generally assumed that there is a large number of reflected signals, with or without a line-of-sight component, which implies that the signal distribution becomes Gaussian, based on the central limit theorem (CLT). For example, if the number of reflected signals is large and there is a line-of-sight component, then the received signal becomes Gaussian with a non-zero mean, and hence, its envelop is Rician. If there is no line-of-sight, the signal mean becomes zero and its envelop is Rayleigh distributed. Nevertheless, in several wireless applications, only a few number of reflected signals are received, and thus, using the Gaussian assumption based on the central limit theorem (CLT) becomes inaccurate, and the widely adopted Rayleigh fading model will not accurately capture the fading effect. In such scenarios, the hyper-Rayleigh fading model would be more accurate and will be more suitable to use [3], [22], [23].

According to hyper-Rayleigh model, the received signal r_n

at the nth user can be written as

$$\begin{aligned} r_n &= \left(\sum_{i=1}^{L} a_{i,n}\cos\phi_{i,n}\right)x + w_n \\ &= h_n x + w_n \\ &= |h_n|\, e^{j\theta_n} x + w_n \end{aligned} \tag{3}$$

where h_n is a complex fading coefficient between the BS and the nth user, $w_n \sim \mathcal{CN}\left(0,\sigma_n^2\right)$ is the additive white Gaussian noise (AWGN), L is the number of specular received components, $\phi_{i,n}$ is the phase of the ith received component and follows uniform distribution, i.e., $\phi_{i,n} \sim \mathcal{U}\left[-\pi,\pi\right]$, and $a_{i,n}$ is the amplitude. Moreover, $\phi_{i,n}$ and $a_{i,n}$ are mutually independent $\forall\{i,n\}$. For a special case where $L \to \infty$, the CLT can be applied, and thus $h_n \sim \mathcal{CN}\left(0,\sigma_{h,n}^2\right)$ follows the complex Gaussian distribution and $\alpha_n = |h_n|$ is Rayleigh distributed random variable. However, h_n generally follows hyper-Rayleigh distribution. For the sake of completeness, the hyper-Rayleigh PDFs for $L = 2$, 3, and 4 are given by [3], [22], [23]:

Two-ray model, $L = 2$:

$$f_\alpha(\alpha) = \frac{2\alpha}{\pi\sqrt{4a_1^2a_2^2 - \left(\alpha^2 - a_1^2 - a_2^2\right)^2}},\ 0 \le \alpha \le a_1 + a_2 \tag{4}$$

Three-ray model, $L = 3$:

$$f_\alpha(\alpha) = \int_0^\pi \frac{2\alpha\ \Phi(1-|\bar{\psi}_3|)\ d\phi_1}{\pi^2\sqrt{4a_3^2\bar{b}_2^2 - (b_3^2 - \bar{b}_2^2 - a_3^2)^2}},\ \check{b}_3 \le \alpha \le \hat{b}_3, \tag{5}$$

where $\Phi(\cdot)$ is the Heaviside step function with $\Phi(0) = 0$,

$$\bar{b}_2^2 \triangleq \|\mathbf{a}_2\|^2 + 2a_1a_2\cos(\phi_1),$$

$$\bar{\psi}_3 \triangleq \frac{\left(\alpha^2 - \bar{b}_2^2 - a_3^2\right)}{2a_3\bar{b}_2},$$

$$\check{b}_L = \max\left\{\left[2\max(\mathbf{a}_L) - \sum_{i=1}^{L} a_i\right], 0\right\},$$

$\|\mathbf{a}_L\|^2 = \sum_{i=1}^{L} a_i^2$, and $\hat{b}_L = \sum_{i=1}^{L} a_i$.

Four-ray model, $L = 4$:

$$f_\alpha(\alpha) = \int_{-\pi}^{\pi}\int_{-\pi}^{\pi} \frac{\alpha\Phi(1-|\bar{\psi}_4|)\ d\phi_1 d\phi_2}{2\pi^3\sqrt{4a_4^2\bar{b}_3^2 - (\alpha^2 - \bar{b}_3^2 - a_4^2)^2}},$$
$$\check{b}_4 \le \alpha \le \hat{b}_4, \tag{6}$$

where

$$\bar{\psi}_4 \triangleq \frac{\left(b_4^2 - \bar{b}_3^2 - a_4^2\right)}{2A_4\bar{b}_3},$$

$$\bar{b}_3^2 = \|\mathbf{a}_3\|^2 + 2a_1a_2\cos(\phi_1) + a_2a_3\cos(\phi_2) + a_1a_3\cos(\phi_2 - \phi_1).$$

Fig. 2 shown the PDF of hyper-Rayleigh random variable for different values of L, where the average power is normalized to 1, i.e., $E\left[\alpha_n^2\right] = 1$, and $a_i = 1\forall i$ is considered. As can be observed from this figure, the PDF for low values of L is very different from Rayleigh, denoted as Rayl., distribution, which implies that the well-known Rayleigh model is not suitable when few components dominate the received signal. However, the PDF of a α_n becomes closer to Rayleigh distribution as the value of L increases.; for example, the distribution when $L = 10$ is almost identical with Rayleigh distribution.

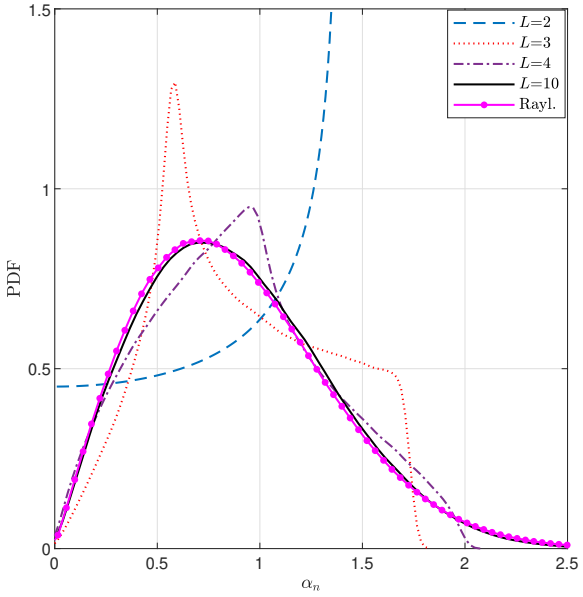

Fig. 2. The distribution of the hyper-Rayleigh with normalized power, i.e., $E\left[\alpha_i^2\right] = 1$, for different values of L.

C. Receiver Model

For coherent detection, the channel phase $\arg\{h_n\} \triangleq \theta_n$ can be estimated and compensated separately from α_n. Given that the channel phase θ_n is estimated and compensated perfectly at the nth UE receiver, then the received signal after phase compensation can be written as

$$\check{r}_n = r_n e^{-j\theta_n},\ \check{r}_n = \alpha_n x + \check{w}_n \tag{7}$$

where $\check{w}_n = w_n e^{-j\theta_n}$. Given that w_n is circularly symmetric, then $\check{w}_n \sim w_n \sim \mathcal{CN}\left(0,\sigma_n^2\right)$. Without loss of generality, we assume that $\alpha_1 < \alpha_2 < \cdots < \alpha_N$, and thus, the power allocation coefficients β_i's are assigned by the BS in the opposite order of channel gains, i.e., $\beta_1 > \beta_2 > \cdots > \beta_N$, to enable satisfying the quality of service (QoS) requirements for far users. Fig. 3 shows an example for a two users NOMA network. Therefore, the channel model for each user follow the order statistics [20]

$$f_{\alpha_n}(\alpha_n) = K_n f(\alpha)\left[F(\alpha)\right]^{n-1}\left[1 - F(\alpha)\right]^{N-n} \tag{8}$$

where $K_n = \frac{N!}{(n-1)!(N-n)!}$, $f(\alpha)$ and $F(\alpha)$ are the PDF and CDF of α, respectively, which corresponds to the hyper-

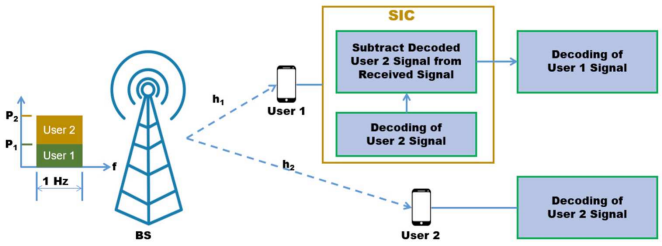

Fig. 3. An example of a BS employs power-domain NOMA to transmit data to two user.

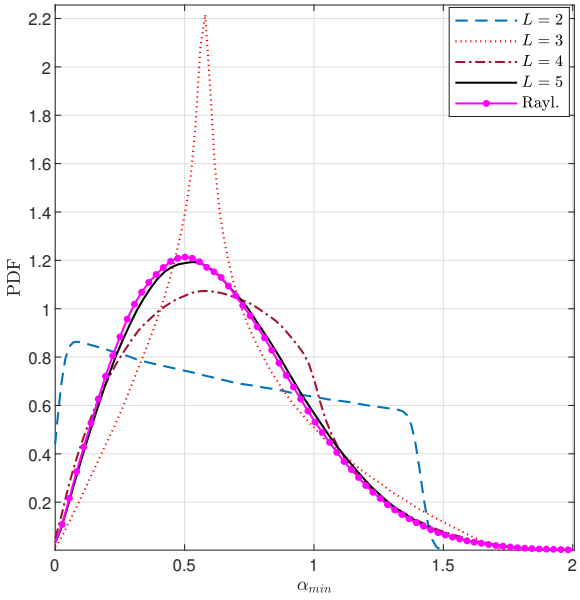

Fig. 4. The distribution of the the ordered channel amplitude $\alpha_{\min}$.

Rayleigh model. Unfortunately, deriving closed-form expressions for $f_{\alpha_n}(\alpha_n)$ given that $f_{\alpha}(\alpha)$ is hyper-Rayleigh is intractable, and hence, numerical analysis or Monte Carlo simulation can be used. Figs. 4 and 5 show $f_{\alpha_1}(\alpha_1)$ and $f_{\alpha_2}(\alpha_2)$, respectively. As can be noted from the figures, the order statistics of the hyper-Rayleigh is significantly different from the Rayleigh for $L \leq 3$.

The detection process at each receiver can be performed using a maximum likelihood detector (MLD), or a SIC detector, which has lower complexity and equivalent performance, and hence, SIC is considered in this work. To extract the information symbols s_n at the nth user equipment, SIC is applied where the signal for the nth user is detected after detecting and subtracting the signals of the first $n-1$ users. Therefore, the maximum likelihood detection (MLD) is applied n times, however, the constellation size in each MLD is equal to the

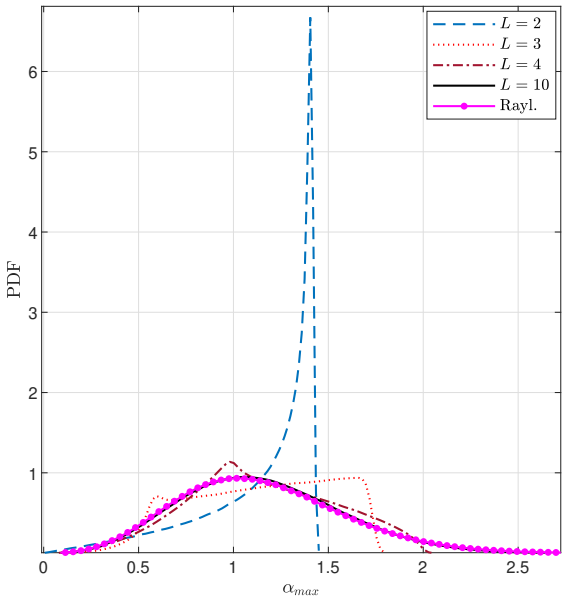

Fig. 5. The distribution of the the ordered channel amplitude $\alpha_{\max}$.

modulation order of the nth user signal, and thus,

$$\hat{s}_n = \arg\min_{\tilde{s}_n} \left| r_n - \hat{h}_n \sum_{i=1}^{n-1} \sqrt{\beta_i}\hat{s}_i - \hat{h}_n \sqrt{\beta_n}\tilde{s}_n \right|^2 . \quad (9)$$

For the two users scenario, as shown in Fig. 3, the far user can detect its own signal directly by considering the multi-user signal as an unknown additive noise. For UE-1, the scenario is different because it has to apply SIC to be able to detect its own signal. According to this detection approach, UE-1 detects the signal of UE-2 first, and then the interference cancellation is performed by subtracting UE-2's signal, and finally UE-1 detects its own signal based on the obtained signal after the interference cancellation.

III. Numerical Results

This section introduces the simulation results for a downlink NOMA system, where Monte Carlo simulation run consists of 10^7 realization. The BS and users use a single antennas and apply Gray coded QPSK constellation. The channel between the BS and each user is modeled as a ordered hyper-Rayleigh flat fading channel with unit power, i.e., $E\left[\alpha_i^2\right] = 1$, and the results are compared with Rayleigh channel. The number of users $N = 2$ and the power allocation is set to $\beta_1 = 0.7$ and $\beta_2 = 0.3$, unless it is specified otherwise.

Fig. 6 presents the BER for the two-ray model, $L = 2$, and compares it to the conventional Rayleigh fading, i.e., $L = \infty$. In this figure we used $a_1 = a_2$ with four different values of a_i, i.e., $a_i \in \{0.25, 0.5, 0.75, 1\}$. As can be noted from this figure, the BER of U_1 is always worse than BER of U_2 in the case of hyper- Rayleigh, while a switch-over occurs for the case of Rayleigh fading. For the cases of $a_i = 0.75$ and $a_i = 1$, the

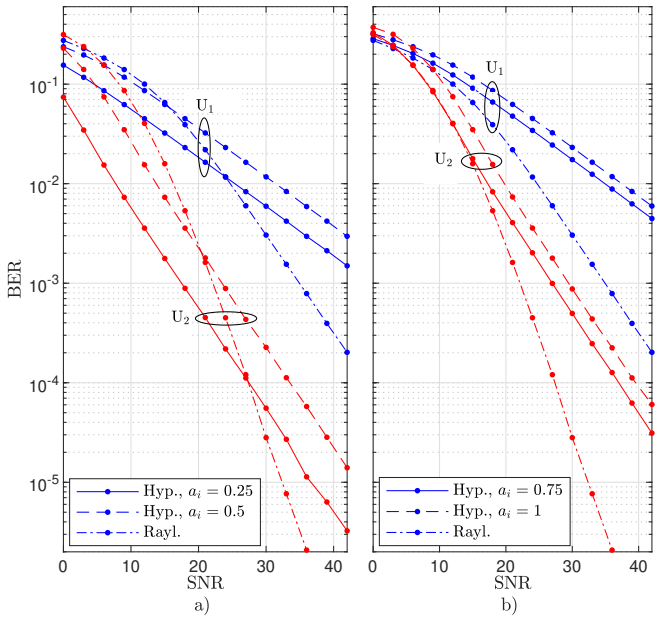

Fig. 6. The probability of bit error for the two-ray model different values of $\{a_1, a_2\}$.

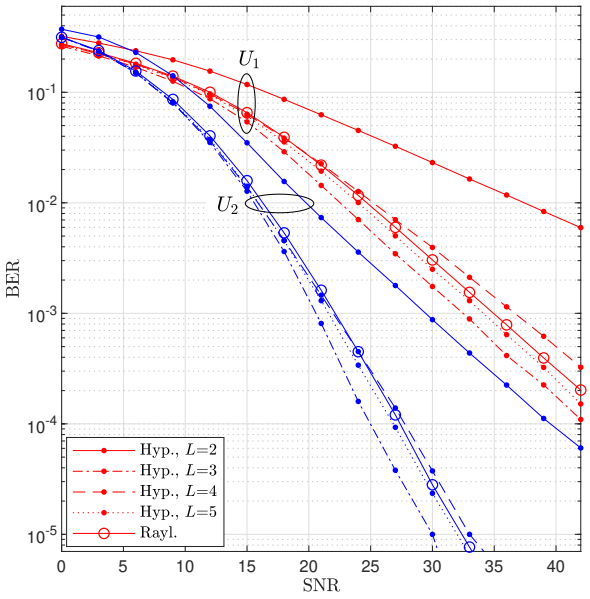

Fig. 7. The BER for a two-user NOMA system for different values of L.

BER under Rayleigh fading is lower than the hyper-Rayleigh for the entire SNR. However, it is not the case when $a_i = 0.25$ or $a_i = 0.5$, where the relative difference depends on SNR. From this figure, it can be concluded that Rayleigh model could be inaccurate when the number of specular components is small.

Fig. 7 shows the BER for a two-user NOMA based communication system for different values of specular components L. The values of a_i for both h_1 and h_2 are taken from the vector $\vec{a_i} = \{1, 0.75, 0.5, 0.25, 0.1\}$, and the results are compared to the case of Rayleigh channel. As can be noted from figure, the BER of U_2 is better than BER of U_1. In addition, the performance under two-ray channel conditions is very different from Rayleigh scenario; however, both models provide comparable BER as the value of L increases. Moreover, it can be noted from the figure that fading severity is not directly proportional to the number of specular components L as the BER fluctuates with different values of L as compared to Rayleigh fading.

Fig. 8 shows the BER using different power allocation coefficients for $L = 2$, where $a_1 = 1$ and $a_2 = 0.75$. It can be observed from the figure that for a given value of β_1, the BER of the near user, i.e., U_2, is better than the BER of the far user, i.e., U_1. For example, the BER of U_2 is better when $\beta_1 = 0.8$ although its allocated power is less than U_1, where the performance loss in the BER of U_1 is due to the long-term fading caused by distance. Another interesting point is that when both user are allocated equal amount of power, i.e., $\beta_1 = 0.5$, both users are not able to recover their signals. It should be noticed that this behavior is due to the large value of interference caused by allocating equal or adjacent values of power for the users.

IV. Conclusion

In this paper, the BER performance of downlink NOMA system was studied under hyper-Rayleigh fading channel, which perfectly captures the situation in which few strong received components dominate the received signal. SIC based detection is applied by users for efficient signal extraction. It has been shown that there is considerable difference in the BER values when hyper-Rayleigh is compared to Rayleigh channel, and thus accurate channel modeling is required when designing NOMA based communication system; for example, Rayleigh model is impractical when the received signal is subject to two-ray (ground ref lection) model. In addition, results showed that power allocation is very critical to provide users adequate QoS in terms of capacity and BER.

Future work may include the BER analysis of NOMA communication under hyper-Rayleigh fading channels. In addition, the optimum power allocation for user equipment which guarantee the QoS requirements for all users including the BER and transmission rate.

Acknowledgment

This work was supported in part by the KU Center for Cyber Physical Systems, in part by the European Union's Horizon 2020 Research and Innovation Programme through the Marie Sklodowska-Curie under Grant 812991, and in part by the Natural Sciences and Engineering Research Council of Canada (NSERC) through its Discovery Program.

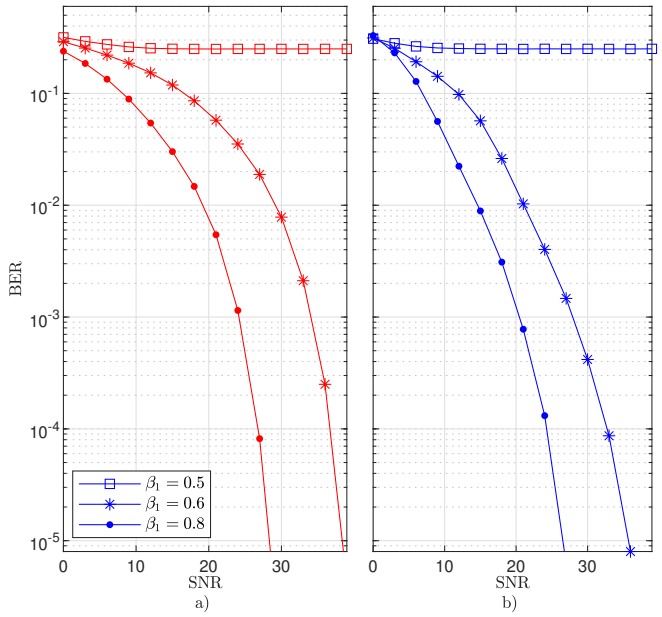

Fig. 8. The BER for different power allocation coefficients, $L = 2$: a) BER for user U_1, b) BER for user U_2.

REFERENCES

[1] "Mobile data traffic outlook." [Online], available: outlookhttps://www.ericsson.com/en/mobility-report/reports/november-2019/mobile-data-traffic-outlook. Accessed 29 Dec. 2019.

[2] Q. Nadeem et al, "Design of 5G full dimension massive MIMO systems," *IEEE Trans. Commun.*, vol. 66, no. 2, pp. 726-740, Feb. 2018.

[3] M. Mirahmadi, A. Al-Dweik, and A. Shami, "Interference modeling and performance evaluation of heterogeneous cellular networks," *IEEE Trans. Commun.*, vol. 62, no. 6, pp. 2132-2144, Jun. 2014.

[4] M. Kalil *et al.*, "A framework for joint wireless network virtualization and cloud radio access networks for next generation wireless networks," *IEEE Access*, vol. 5, pp. 20814–20827, 2017.

[5] M. Kalil *et al.*, "Efficient low complexity scheduler for wireless resource virtualization," *IEEE Wireless Commun. Lett.*, vol. 5, no. 1, pp. 56–59, Feb. 2016.

[6] M. Kalil, *et al.*, "Low-complexity power-efficient schedulers for LTE uplink with delay-sensitive traffic," *IEEE Trans. Veh. Technol.*, vol. 64, no. 10, pp. 4551-4564, Oct. 2015.

[7] M. Morant *et. al*, "Experimental demonstration of mm-wave 5G NR photonic beamforming based on ORRs and multicore fiber," *IEEE Trans. Microw. Theory Techn.*, vol. 67, no. 7, pp. 2928-2935, July 2019.

[8] M. Al-Jarrah *et al.*, "Error rate analysis of amplitude-coherent detection over Rician fading channels with receiver diversity," *IEEE Trans. Wireless Commun.*, IEEE Xplore early access, doi: 10.1109/TWC.2019.2942588, Sep. 2019.

[9] Z. Huang *et al.*, "Hybrid optical wireless network for future SAGO-integrated communication based on FSO/VLC heterogeneous interconnection," *IEEE Photon. J.*, vol. 9, no. 2, pp. 1-10, Apr. 2017.

[10] Q. Sun, S. Han, C. I, and Z. Pan, "On the ergodic capacity of MIMO NOMA systems," *IEEE Wireless Commun. Lett.*, vol. 4, no. 4, pp. 405-408, Aug. 2015.

[11] J. Kim and I. Lee, "Capacity analysis of cooperative relaying systems using non-orthogonal multiple access," *IEEE Commun. Lett.*, vol. 19, no. 11, pp. 1949-1952, Nov. 2015.

[12] Y. Liu *et al.*, "On the capacity comparison between MIMO-NOMA and MIMO-OMA," *IEEE Access*, vol. 4, pp. 2123-2129, 2016.

[13] J. Kim, I. Lee, and J. Lee, "Capacity scaling for D2D aided cooperative relaying systems using NOMA," *IEEE Wireless Commun. Lett.*, vol. 7, no. 1, pp. 42-45, Feb. 2018.

[14] Z. Yang *et al.*, "Outage performance for dynamic power allocation in hybrid non-orthogonal multiple access systems," *IEEE Commun. Lett.*, vol. 20, no. 8, pp. 1695-1698, Aug. 2016.

[15] X. Wang *et al.*, "Outage analysis for downlink NOMA with statistical channel state information," *IEEE Wireless Commun. Lett.*, vol. 7, no. 2, pp. 142-145, Apr. 2018.

[16] S. Xie *et al.*, "Outage performance of NOMA-based integrated satellite-terrestrial networks with imperfect CSI," *Electron. Lett.*, vol. 55, no. 14, pp. 793-795, Jul. 2019.

[17] L. Bariah, S. Muhaidat, and A. Al-Dweik, "Error probability analysis of non-orthogonal multiple access over Nakagami-m fading channels," *IEEE Trans. Commun.*, vol. 67, no. 2, pp. 1586–1599, Feb. 2019.

[18] F. Kara and H. Kaya, "Performance analysis of SSK-NOMA," *IEEE Trans. Veh. Technol.*, vol. 68, no. 7, pp. 6231–6242, Jul. 2019.

[19] L. Bariah, S. Muhaidat, and A. Al-Dweik, "Error probability analysis of NOMA-based relay networks with SWIPT," *IEEE Commun. Lett.*, vol. 23, no. 7, pp. 1223–1226, Jul. 2019.

[20] T. Assaf *et al.*, "Exact BER performance analysis for downlink NOMA systems over Nakagami-m fading channels," *IEEE Access*, vol. 7, pp. 134539-134555, 2019.

[21] M. S. Ali *et. al*, "Downlink power allocation for CoMP-NOMA in multi-cell networks," *IEEE Trans. Commun.*, vol. 66, no. 9, pp. 3982-3998, Sep. 2018.

[22] Y. Maghsoodi and A. Al-Dweik, "Error-rate analysis of FHSS networks using exact envelope characteristic Functions of sums of stochastic signals," *IEEE Trans. Veh. Technol.*, vol. 57, no. 2, pp. 974-985, Mar. 2008.

[23] A. Al-Dweik, B. Sharif, and C. Tsimenidis, "Accurate BER analysis of OFDM systems over static frequency-selective multipath fading channels," *IEEE Trans. Broadcast.*, vol. 57, no. 4, pp. 895-901, Dec. 2011.